ELASTIC AND TOTAL $\pi^+\pi^-$ CROSS SECTIONS FROM A HIGH STATISTICS MEASUREMENT OF THE REACTION $\pi^-p \to \pi^+\pi^-n$ AT 63 GeV/c

C. Daum, L. Hertzberger, W. Hoogland, S. Peters, P. Van Deurzen,
NIKHEF-H, Amsterdam, The Netherlands.

A. Berglund, V. Chabaud, B. Hyams, H. Tiecke, P. Weilhammer,
CERN, Geneva, Switzerland.

A. Dwurazny, H. Palka, G. Polok, K. Rybicki, M. Turala, J. Turnau, A. Zalewska,
Institute of Nuclear Physics, Cracow, Poland.

H. Becker, G. Blanar, M. Cerrada, H. Dietl, J. Gallivan, M. Glaubman, R. Klanner, E. Lorenz, G. Lütjens, G. Lutz, W. Männer, U. Stierlin,
Max Planck Institute, Munich, Germany.

I. Blakey, M. Bowler, R. Cashmore, J. Loken, J. Spalding, G. Thompson,
Nuclear Physics Laboratory, University of Oxford, Oxford, U.K.

B. Alper, C. Damerell, A. Gillman, J. Hardwick, F. Wickens,
Rutherford Laboratory, Chilton, Didcot, Oxfordshire, U.K.

(Presented by P. Weilhammer)

ABSTRACT

A sample of about 230 000 events of the reaction $\pi^-p \to \pi^+\pi^-n$, measured with a magnetic forward spectrometer set up in an unseparated π^- beam with a momentum of 63 GeV/c at the SPS has been analysed in terms of one pion exchange. The elastic $\pi^+\pi^-$ cross section has been determined using an extrapolation to the pion pole in the mass range up to $m_{\pi^+\pi^-} = 4$ GeV. The total $\pi^+\pi^-$ cross section is obtained via the optical theorem.

1. INTRODUCTION

A large acceptance forward wire chamber spectrometer using two large magnets was set up in a hadron beam at the SPS. Besides a number of other exclusive and inclusive channels, the reaction

$$\pi^-p \to \pi^+\pi^-n \qquad (1)$$

was studied at 63.2 GeV beam energy. The purpose of this measurement was twofold: (i) to study the production mechanism of resonances in the $\pi^+\pi^-$ system up to high momenta and large momentum transfers, and (ii) to investigate $\pi^+\pi^-$ scattering at the highest attainable $\pi^+\pi^-$ centre-of-mass energies.

In this paper we report first results from a determination of elastic and total $\pi^+\pi^-$ cross sections obtained from a sample of more than 60 000 events with a mass $m_{\pi^+\pi^-} \geq 2.0$ GeV. A comparison with the features of $\bar{p}p$ scattering is given.

2. APPARATUS AND TRIGGER

A schematic layout of the spectrometer is shown in Fig. 1. The essential feature of the spectrometer is the use of two large aperture forward magnets in series. The first one, with a gap of $260 \times 60 \times 90$ cm^3 and a bending power of 9 kGm, analyses the momentum of low

energy particles in the range from 300 MeV to about 3 GeV with good acceptance and the second one with a gap of $150 \times 50 \times 110$ cm^3 and a bending power of 20 kGm, provides an accurate momentum measurement for particles up to 100 GeV. Before and after the first magnet 24 and 20 planes of wire spark chambers (I and II) (0.25 mm resolution/plane) gave an accurate determination of particle trajectories. There were a further 18 planes of large wire chambers (IIIa,IIIb,IIIc) arranged in three groups and interspaced by two large Čerenkov (Č1,Č2) hodoscopes behind the second magnet. The 50 cm long liquid H_2 target was surrounded by a barrel of Pb scintillator sandwich anticoincidence counters (F) with only a small hole upstream for the beam to enter and a rectangular exit window matching the magnet apertures to let the forward moving secondary particles pass. Three further arrays of Pb scintillator sandwich counters (G,H) were installed downstream from the target to redefine windows. The gap of the first magnet was also lined with Pb scintillator sandwich counters.

Two 32 element counter arrays (P2/3) behind the first magnet and a set of two proportional wire chamber planes (P1), one with vertical wires and the other with 15^o inclined wires (1 mm pitch), set up directly behind the target, could be used for selecting a desired multiplicity of secondary charged particles. The direction of the incoming beam was determined by a set of 10 proportional wire chamber planes. Two standard CEDAR Čerenkov counters and one threshold Čerenkov counter served for efficient discrimination of incoming π's, K's, and protons in the beam. A telescope of five scintillation counters was used to define the incoming beam. A small scintillation counter D_2 after the second magnet could be used to signal non-interacting beam particles.

The trigger condition for the selection of reaction (1) was an incoming negatively-charged particle, selected by the beam counters and two charged particles in the forward direction defined by two hits in either one of the two proportional wire planes P1 and two hits in the counter array P2/3 with back-to-back counters in P2 and P3 in coincidence. This trigger condition is however not yet sufficient to select reaction (1) efficiently since there is a very high electromagnetic background of forward two-prongs caused by a beam and a knock-on electron with an energy above 300 MeV, most frequently produced in the H_2 target. An anticoincidence signal from the D_2 counter cannot be used in the trigger since this would veto forward going π^-'s from reaction (1), which comprise a large fraction of the high mass $\pi^+\pi^-$ events. We therefore applied a special anticoincidence logic to eliminate these knock-on electrons, making use of the fact that those δ-electrons are emitted with a very small opening angle with the beam and therefore all arrive at one side of the counter array P2/3 behind the first magnet. Two-prong events, having a coincidence hit in the central P2/3 element (on which the beam was focused) and in the D_2 counter, in addition to a hit on any one element on the "negative" side of the P2/3 array were rejected.

Additionally, all anticoincidence signals from the counters F, G and H vetoed the trigger in order to reject events with additional charged or neutral particles outside the solid angle defined by the magnet apertures. In this way the trigger rate was cut down to an acceptable level ($\sim$20 triggers per 10^5 incoming beam particles).

3. DATA PROCESSING AND EVENT SELECTION

A total of about $5.8 \cdot 10^6$ triggers, including calibration runs for determining losses of

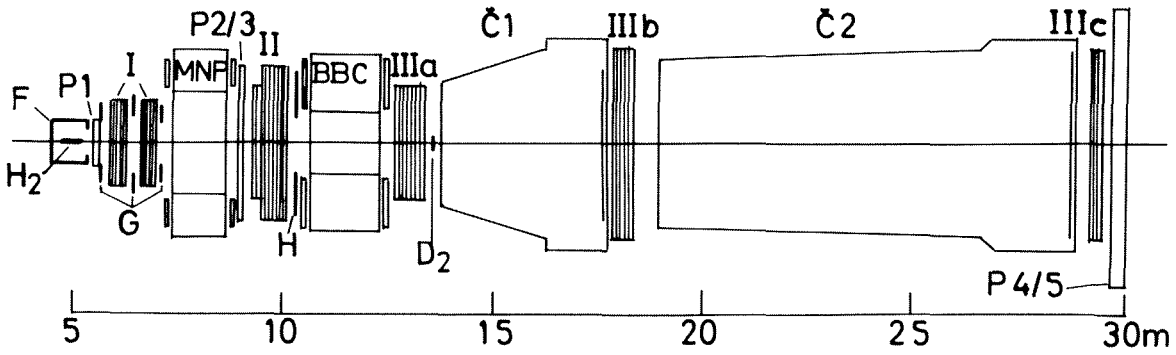

Fig. 1 Schematic layout of the WA3-Spectrometer.
H_2 : Hydrogen Target; MNP,BBC : Spectrometer Magnets;
I,II,IIIa,b,c : 80 planes of Wire Spark chambers;
P1 : MWPC's:, P2/3 : 32 element counter arrays;
F,G,H,D,P4/5 : Pb-Scintillator-Sandwich Veto Counters;
Č1,Č2 : Hodoscopic Threshold Čerenkov Counters.

good events caused by the trigger conditions, were recorded. All events were processed through a geometry and kinematics program which had about 98% efficiency to fully reconstruct events with two charged forward going particles. After appropriate cuts applied in order to select a clean sample of events of reaction (1) we obtained about 230 000 good $\pi^+\pi^-$ events. In Fig. 2a the mass spectrum is shown for the observed events and after acceptance corrections (see chapter 4). In the following we will concentrate on the data in the high mass region.

4. METHOD OF ANALYSIS

The raw data shown in Fig. 2a have to be corrected for geometrical acceptance losses. The $\pi^+\pi^-$ events are characterized by the following parameters:

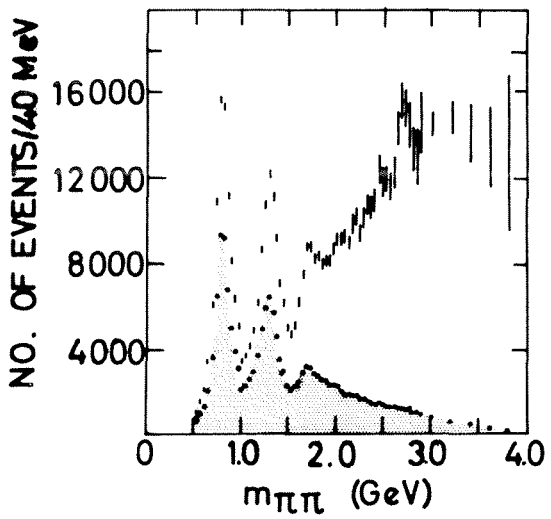

Fig. 2a $\pi^+\pi^-$ Mass Spectrum
dots : observed
lines : acceptance corrected

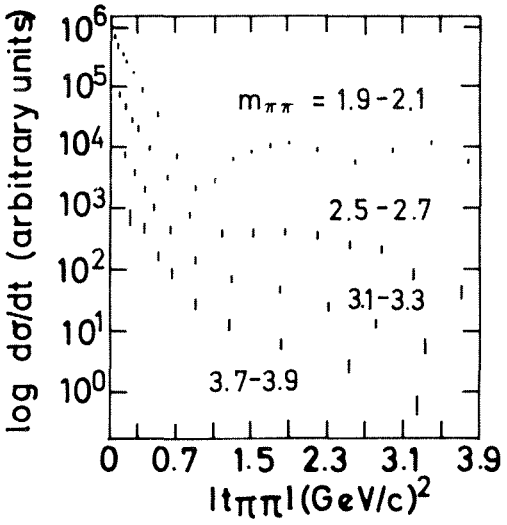

Fig. 2b Differential $\pi^+\pi^-$ Cross Sections $\frac{d\sigma^{\pi\pi}}{dt_{\pi\pi}}$ for 4 different $m_{\pi^+\pi^-}$ mass intervals

$m_{\pi^+\pi^-}$: rest mass of the $\pi^+\pi^-$ system

t_{pn} : four momentum transfer to the nucleon

$\cos\theta,\phi$: decay angles of the π^- in the $\pi^+\pi^-$ rest system in the t-channel helicity frame

$t_{\pi\pi} = -2q^2(1-\cos\theta)$ is the four momentum transfer between the incoming and outgoing π^-

$q = \frac{1}{2}\sqrt{m^2_{\pi\pi} - 4m^2_{\pi}}$ -- momentum of each pion in the centre-of-mass of the $\pi^+\pi^-$ system.

The geometrical acceptance of the $\pi^+\pi^-$ events is calculated by a Monte Carlo method. Events are generated at fixed $m_{\pi^+\pi^-}$, t_{pn} values isotropically in ϕ. Since the observed events exhibit a strongly forward peaked $\cos\theta$ distribution, in particular at high $\pi\pi$ masses, the Monte Carlo events have been generated with a $\cos\theta$ distribution derived from the observed events. In this way we ensure that the statistical error of the Monte Carlo calculation is small compared to the error on the observed events over the whole $\cos\theta$ range using the minimal computer time necessary.

At higher dipion masses ($m_{\pi\pi} \lesssim 2$ GeV) we observe $t_{\pi\pi}$-distributions which show more and more a forward-peaked diffractive pattern. A description of this distribution in terms of moments of spherical harmonics needs too many high order terms to be practical. Therefore the $\cos\theta$ distribution was fitted independently in 20 $\cos\theta$-bins of varying bin size.

Our data show that spherical harmonics moments $\langle Y_{\ell m}\rangle$ with $m \geq 2$ are negligible for $|t_{pn}| \lesssim 0.2$ GeV^2. It is therefore possible to describe the ϕ-dependence of the double differential cross section by

$$\frac{d^2\sigma}{d\cos\theta d\phi} = I_0(\cos\theta) + I_1(\cos\theta) \cdot \cos\phi \qquad (2)$$

In a first step this expression is fitted in given $m_{\pi\pi}, t_{pn}$ intervals in each of 20 $\cos\theta$ bins using a least squares method ($\Delta m_{\pi\pi} = 0.2$ GeV, $0 < |t_{pn}| < 0.2$ GeV^2).

The resulting I_0, I_1 are used as input to a maximum likelihood program in which the I_0, I_1 of (2) are also parametrized as functions of t_{pn}.

These parametrizations can be derived from a generalization of the poor man's absorption model[1] by Ochs and Wagner[2]

$$I_0 = \frac{-t_{pn}}{(m_\pi^2 - t_{pn})^2} F_0^2(t_{pn}) |T|^2 + \frac{|C_A|^2}{m^2_{\pi\pi}} F_1^2(t_{pn}) \left|\frac{dT}{d\theta}\right|^2 \qquad (3)$$

$$I_1 = \frac{\sqrt{-t_{pn}}}{(m_\pi^2 - t_{pn})} F_0(t_{pn})\, F_1(t_{pn})\, \mathrm{Re}\, \frac{C_A}{m^2_{\pi\pi}} \frac{d}{d\theta} |T|^2 \qquad (4)$$

$T(m_{\pi\pi},\cos\theta)$ is the $\pi\pi$ scattering amplitude

C_A is the absorption strength parameter

$F_i(t)$ form factors

These formulae contain the required small $t_{\pi\pi}$-behaviour

$$I_1 \propto \sin\theta \propto \sqrt{-t_{\pi\pi}} \qquad (5)$$

and for the second term in I_0

$$I_0^{(2)} \propto \sin^2\theta \propto |t_{\pi\pi}| \quad .$$

We assume C_A to be real. Preliminary fits using a Regge-type parametrization showed that the second term in formula (3) $I_0^{(2)}$ is smaller than 10% over the whole $t_{\pi\pi}$-region. In the small $t_{\pi\pi}$-region which is used to extract the total $\pi\pi$ cross section it vanishes $\propto|t_{\pi\pi}|$. From this contribution we therefore expect a contamination of the elastic $\pi\pi$-cross section of less than 10%. Its contribution to the total cross section can be neglected.

We incorporate in our fits the minimal contribution only which is obtained by neglecting a relative phase change between T and $\frac{dT}{d\theta}$.

We take $F_0^2(t_{pn}) = F_1^2(t_{pn}) = e^{b(t_{pn}-m_\pi^2)}$ and obtain

$$\begin{aligned} I_0 &= \frac{-t_{pn}}{(m_\pi^2 - t_{pn})^2}\, e^{b(t_{pn}-m_\pi^2)} \cdot T_0^2 + e^{b(t_{pn}-m_\pi^2)} \cdot \frac{1}{4} T_1^2 \\ I_1 &= \frac{\sqrt{-t_{pn}}}{m_\pi^2 - t_{pn}}\, e^{b(t_{pn}-m_\pi^2)} \cdot T_0 \cdot T_1 \end{aligned} \qquad (6)$$

where $T_0 = |T|$

$$T_1 = \frac{2C_A}{m_{\pi\pi}} \left|\frac{dT}{d\theta}\right|$$

T_0, T_1 are again fitted independently in 20 $\cos\theta$ bins, the slope b is taken to be the same for all $\cos\theta$ in a given $m_{\pi\pi}$ bin. We do not demand $T_1 \propto \frac{dT}{d\theta}$ in our fits.

Using the Chew-Low formula

$$\lim_{(t_{pn} \to m_\pi^2)} \frac{d^3\sigma}{dm_{\pi\pi}\, dt_{pn}\, d\cos\theta} = \frac{m_{\pi\pi}^2\, q_\pi}{4\pi\, m_p^2\, p_{Lab}^2} \frac{g^2}{4\pi} \frac{-t_{pn}}{(m_\pi^2 - t_{pn})^2}\, e^{b(t_{pn}-m_\pi^2)} \frac{d\sigma_{\pi\pi}^{el}}{d\cos\theta}$$

one obtains directly the pole-extrapolated elastic $\pi\pi$-cross section

$$\frac{d\sigma_{\pi\pi}^{el}}{d\cos\theta} = T_0^2 \Big/ \left(\frac{m_{\pi\pi}^2\, q_\pi}{4\pi\, m_p^2\, p_{Lab}^2} \cdot \frac{g^2}{4\pi} \right)$$

where p_{Lab} = beam momentum
$g^2/4\pi$ = 2×14.6 = pion nucleon coupling constant
m_p = mass of proton .

In Fig. 2b the fitted values T_0^2 are shown for four $m_{\pi\pi}$ mass bins ($1.9\ \text{GeV} < m_{\pi\pi} < 2.1\ \text{GeV}$, $2.5\ \text{GeV} < m_{\pi\pi} < 2.7\ \text{GeV}$, $3.1\ \text{GeV} < m_{\pi\pi} < 3.3\ \text{GeV}$ and $3.7\ \text{GeV} < m_{\pi\pi} < 3.9\ \text{GeV}$) as a function of $t_{\pi\pi}$. This pole extrapolated differential $\pi^+\pi^-$ cross section follows an exponential in the $|t_{\pi\pi}|$ interval $0 < |t_{\pi\pi}| < 0.7\ \text{GeV}^2/c^2$ for all $m_{\pi\pi}$ mass bins.

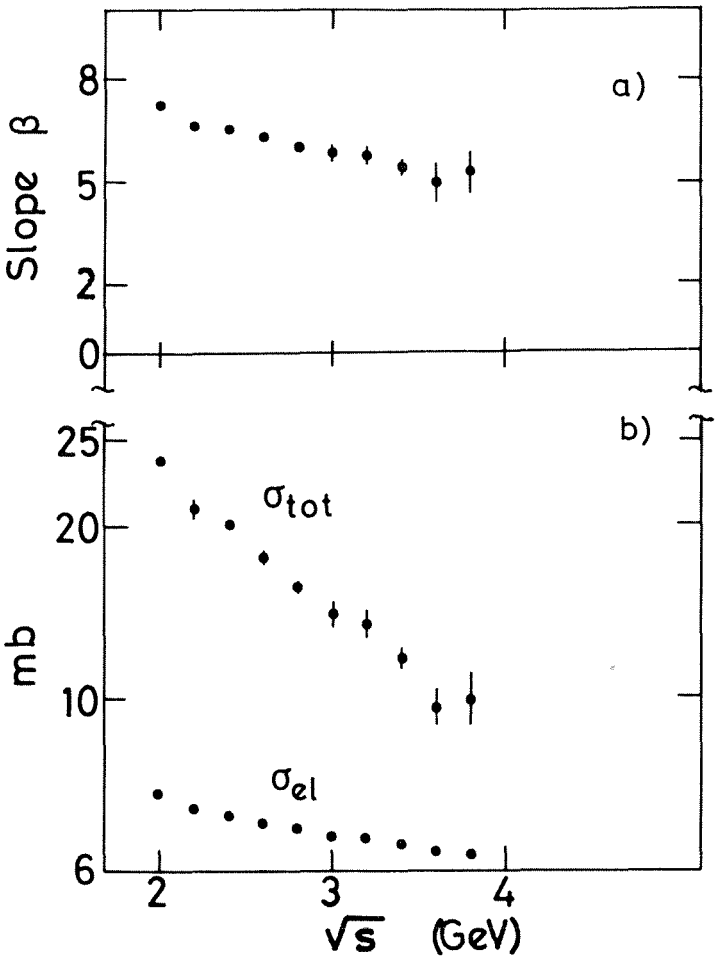

Fig. 3a Slope of $\frac{d\sigma^{\pi\pi}}{dt_{\pi\pi}}$ fitted in the interval $0 < t_{\pi\pi} < 0.7$ $(GeV/c)^2$

Fig. 3b Total and Elastic $\pi^+\pi^-$ cross sections. Errors are statistical only.

The value of the forward $\pi^+\pi^-$ elastic cross section was then determined by fitting an exponential $A\, e^{\beta t_{\pi\pi}}$ to these distributions in each $m_{\pi\pi}$ bin. The values for the slope parameters as a function of $m_{\pi\pi}$ are shown in Fig. 3a.

The total $\pi^+\pi^-$ cross section can now be determined through the optical theorem assuming that the $\pi\pi$ scattering amplitude is purely imaginary in the forward direction. The values thus obtained together with the elastic $\pi^+\pi^-$ cross section, which is calculated by integrating the distribution T_0^2 over $\cos\theta$, are shown in Fig. 3b as a function of $\sqrt{s} = m_{\pi\pi}$. The errors shown in Fig. 3b are statistical only. We estimate in this preliminary analysis the systematic error on the elastic cross section to be 40%, giving an error of 20% for the total cross section. This systematic error is due to uncertainties in the procedure of the extrapolation to the pion pole, of the extrapolation to $t_{\pi\pi} = 0$ and also to the preliminary status of the absolute cross section normalization. We believe that we might be somewhat too low in our cross section due to these systematic effects, since the total cross section at the ρ-meson peak, evaluated in the same way, comes out about 10% below the unitarity bound.

5. DISCUSSION OF RESULTS

The following major features of high energy $\pi^+\pi^-$ collisions in the energy range from $\sqrt{s}$ = 2 GeV to 4 GeV can be observed in our data:

(i) the total cross section still decreases very strongly in the observed energy interval (from about 25 mb to 10 mb). This indicates that $\pi^+\pi^-$ scattering at these energies is not yet purely diffractive.

(ii) The elastic $\pi^+\pi^-$ cross section is decreasing even more strongly than $\sigma_{\pi\pi}^{tot}$ as a function of $\sqrt{s}$. Its value varies from 20% to 10% of the total cross section.

(iii) The elastic differential $\pi^+\pi^-$ cross section follows an exponential shape at low $|t_{\pi\pi}|$. The slope exhibits antishrinkage ($\beta \simeq 7$ (GeV/c)$^{-2}$ at $\sqrt{s}$ = 2 GeV and $\beta \simeq 5$ (GeV/c)$^{-2}$ at $\sqrt{s}$ = 4 GeV).

(iv) The differential cross section has a marked dip around $t = 1$ (GeV/c)^2 at low $\sqrt{s}$, which disappears at higher $\sqrt{s}$.

Around $\sqrt{s}$ = 2 GeV our measured $\sigma_{\pi\pi}^{tot}$ and $\sigma_{\pi\pi}^{el}$ agree with results from a previous bubble chamber experiment[3] at 25 GeV/c. At higher $\sqrt{s}$ our cross section values continue to decrease, whereas Ref. 3 claims a flattening off to a constant value around $\sqrt{s}$ = 3 GeV. One should, however, note that the data sample of Ref. 3 consisted of only about 500 events above $m_{\pi^+\pi^-}$ = 2 GeV.

A comparison with the only other measured hadron-antihadron scattering process, $\bar{p}p \to \bar{p}p$, in the equivalent energy range of $E_{\bar{p}}^{Lab}$ = 3 GeV to 8.5 GeV, shows a very similar pattern: $\sigma_{\bar{p}p}^{tot}$ falls from about 80 mb to 55 mb, the slope of $d\sigma^{\bar{p}p}/dt$ is about twice as large as the slope of $d\sigma^{\pi\pi}/dt$ and also exhibits antishrinkage ($\beta^{\bar{p}p} \simeq 14$ (GeV/c)$^{-2}$ to 12.5 (GeV/c)$^{-2}$) and the ratio $\sigma^{el}/\sigma^{tot} \simeq 20\%$. One also finds the same dip structure in $d\sigma^{\bar{p}p}/dt$ at low $E_{\bar{p}}^{Lab}$ around $t = 0.4$ (GeV/c)^2.

Interpreting the $\pi^+\pi^-$ cross section in terms of an optical model with $\sigma^{tot} \sim R^2$, R representing the extension of the target, indicates that the radius of the pion is about $\frac{1}{2}$ times the radius of the nucleon ($R_\pi \simeq \frac{1}{2}$ fm). From Regge theories[4,5,6] one expects, if factorization is valid, that at very high energies $\sigma_{\pi^+\pi^-} = \frac{\sigma_{\pi^-p}}{\sigma_{pp}}$. Taking our highest energy points one gets $\sigma_{\pi^+\pi^-} = \frac{(27\text{ mb})}{(40\text{ mb})} \simeq 18$ mb, which does not agree with our measured value of 9.7 mb. Predictions based on a model of scattering between the constituent quarks in the different particles[7] give $\sigma_{\pi^+\pi^-} = \frac{2(\sigma_{\pi^-p})^2}{\sigma_{pp}+\sigma_{\bar{p}p}} \simeq 14$ mb, $\beta_{\pi\pi} = 5.8$ (GeV/c)$^{-2}$ and $R_\pi = 0.65$ fm, somewhat higher than our measured values for these quantities.

6. CONCLUSIONS

We have analysed reaction (1) in terms of $\pi^+\pi^-$ scattering for masses $m_{\pi^+\pi^-} \geq 2$ GeV. We find that the $\pi^+\pi^-$ differential, the integrated elastic and the total cross sections have similar energy dependences as observed in $\bar{p}p$ scattering at equivalent energies. The geometrical extension of the pion, as defined in optical models, comes out about 0.5 fm. The values of the total $\pi\pi$ cross section and the exponential slope of the differential cross section are lower than predictions of both the Regge model and the quark model of high energy $\pi\pi$ scattering.

REFERENCES

1) P.K. Williams, PR D1 (1970) 1 12.

2) W. Ochs and F. Wagner, PL 44 B (1973) 271; F. Wagner, NP B58 (1973) 494.

3) W.L. Robertson et al., PR D7 (1973) 9.

4) V.N. Gribov and I. Pomerantchuk, PRL 8 (1962) 343.

5) M. Gell-Mann, PRL 8 (1962) 263.

6) W. Abbe, PR 160 (1967) 1519.

7) E. Strauner, PRL 20 (1968) 1258.